Optics Communications 382 (2017) 162–166

Contents lists available at ScienceDirect

Optics Communications

journal homepage: www.elsevier.com/locate/optcom

Numerical analysis of a photonic crystal fiber based on a surface plasmon resonance sensor with an annular analyte channel

Chao Liu [a,*], Lin Yang [a], Weiquan Su [a], Famei Wang [a], Tao Sun [b], Qiang Liu [a], Haiwei Mu [a], Paul K. Chu [c]

[a] School of Electronics Science, Northeast Petroleum University, Daqing 163318, PR China
[b] Institute of Microelectronics, Agency of Science, Technology and Research (A*STAR), Singapore 117685, Singapore
[c] Department of Physics and Materials Science, City University of Hong Kong, Tat Chee Avenue, Kowloon, Hong Kong, China

ARTICLE INFO

Article history:
Received 29 March 2016
Received in revised form
4 July 2016
Accepted 11 July 2016

Keywords:
Photonic crystal fiber
Surface plasmon resonance
Sensor
Finite element method

ABSTRACT

A sensing structure is designed with a photonic crystal fiber based on a surface plasmon resonance (PCF-SPR) sensor using gold as the sensitive material. The benefit of the structure is to reduce the difficulty in gold deposition, because the Au film is deposited on the outside of the fiber core instead of on the holes filled with analyte inside the core. The properties of the sensor are numerically calculated by the finite element method. The results show that the thickness of the gold film, refractive index of the analyte, and radius of the central hole affect the sensing performance of the PCF-SPR. By optimizing the model, an extra graphene layer with the thickness of 20 nm is deposited on the gold film in the model. The maximum spectral sensitivity can be as high as 7500 nm/RIU for the sensor with the gold-graphene composite film as the sensitive material.

1. Introduction

Monitoring and prevention of disease, food safety, drug testing and environmental pollution are among the most significant issues in the world and a variety of sensors such as resonant rings and disks [1–5], slot waveguides [6,7], and interferometers [8–10] have been employed in the areas mentioned above. Among the different sensing techniques, surface plasmon resonance (SPR) has attracted much attention because of high sensitivity, label-free monitoring, and rapid real-time detection [11].

SPR is a unique optical phenomenon arising from optical excitation of charge-density oscillations localized at the interface between a metallic layer and dielectric surface under a p-polarized light radiation [12]. The prominent feature of SPR sensors is the excellent sensitivity to variations in refractive indexes of the surrounding dielectrics. In the past decade, numerous SPR sensors have been developed in terms of angle modulation based on prisms and wavelength modulation with optical fibers [13]. However, the conventional SPR sensors based on prism-coupled configuration suffer from drawbacks such as high cost, large component size, as well as incompatibility with other systems [14]. Recently, the concept of a photonic crystal fiber (PCF) based SPR sensor has been proposed and it is derived from coupling of a leaky core mode to the plasmonic mode along a metalized fiber micro-structure [15]. These sensors possess excellent characteristics such as a small size, low propagation loss, and high sensitivity thereby overcome the shortcomings of conventional SPR sensors. In particular, a PCF-SPR sensor can achieve a perfect match between the plasmonic mode and core-guided mode, because the effective refractive index of the fundamental mode can be designed to be between zero and the refractive index of the core materials [16].

Several PCF-SPR sensors with different micro-structures have been designed and numerically analyzed. For instance, Hautakorpi et al. have described a three-hole photonic crystal fiber SPR sensor with a gold film deposited on the inner wall of the three holes [17]. Shuai et al. have produced a PCF-SPR sensor with six identical liquid cores surrounded by air holes and the gold film is deposited on the outer wall of the central analyte channel [18]. Recently, efforts have been made to prepare PCF-SPR sensors with graphene-silver composites [19] and silver nanowires [20] as the sensitive materials. The majority of PCF-SPR sensors available consist of large micro-fluidic channels [21] and metalized analyte channels [22]. The key design strategy of PCF-SPR sensors is to ensure efficient coupling between the core-guided mode and plasmonic mode by optimizing the structure. From the perspective of device fabrication, it is difficult to deposit thin metal films on the internal wall of the central small hole in the PCF due to the small curvature. Based on this design concept, several PCF-SPR sensors with large size analyte channels have been proposed and

* Corresponding author.
E-mail address: msm-liu@126.com (C. Liu).

http://dx.doi.org/10.1016/j.optcom.2016.07.031
0030-4018/

reported in recent years [23–25]. In these publications, the sensors consist of two or four metalized large micro-fluidic slots, and their spectral sensitivity in theory is lower than 4000 nm/RIU, which may be limited from intrinsic structures of the sensors. In 2012, Popescu et al. [26] put forward an optical fiber sensor with a large circular gold film and an analyte channel in outermost layer, leading to a substantial simplification in the sensor fabrication. In 2014, Popescu et al. [27] further improved sensing configuration of microstructured plasmon optical fiber and four additional smaller air holes were infiltrated between large air holes, thus giving rise to two sensitive core modes and a significant modification in the propagation parameters of the device. It is also well-known that the performances of PCF-SPR sensors are remarkably dependent on structures of the sensors. A little structure change may lead to remarkable performance variations. Therefore, it is crucial to investigate the influence of structures on performances of the PCF-SPR sensors and further numerical calculation is a necessary step for the design of high-sensitivity PCF-SPR sensors.

Herein, we describe a PCF-SPR sensor with a sensitive film deposited on the outermost layer of the core and the analyte channel is designed to be annular and close to the sensitive film. The performance of the sensor with gold as the sensitive material is assessed numerically and our results reveal a high spectral sensitivity of up to 4875 nm/RIU. Furthermore, graphene layers with a thickness of 20 nm are attempted to be added to the optimized model, which is based on the fact that the large surface area and rich π conjugation structure of graphene makes them suitable dielectric top layers for SPR sensing [28,29]. The sensitivity of the sensor with graphene-gold composite layer as the sensitive material is obviously improved and an extremely higher spectral sensitivity of 7500 nm/RIU is obtained.

2. Theoretical model

The schematic diagram of the PCF-SPR sensor with an annular-shaped analyte channel is depicted in Fig. 1. The Comsol Multiphysics based on the finite element method (FEM) is employed in the numerical evaluation. Free triangles are used to mesh the computational domain. In this study, the number of degrees which can be solved by the software is 62,751 and the number of boundary elements is 1016.

The PCF-SPR sensor comprises four parts. The innermost part is silica with seven air holes arranged hexagonally. As the holes reduce the refractive index of pure silica, the phase matching condition between the fundamental mode and plasmonic mode can be guaranteed. The thin gold film and analyte channel are designed as the second and third layers, respectively. The perfectly matched layer (PML) [30] is the outermost layer and radiation absorber. The radius of the central air hole and cladding air hole are $r_1=0.4$ μm and $r_2=0.6$ μm, respectively, and $n=1.0$ is the refractive index of air. The distance between adjacent air holes is $d=3$ μm and the thicknesses of the gold film and analyte layer are $t_{Au}=0.05$ μm and $t_{anal}=0.4$ μm, respectively. The radius of gold layer is $r_{Au}=4.05$ μm. The refractive index of the silica glass is fixed at 1.45 and the refractive index of analyte varies from 1.33 to 1.42. The electric constant of gold is determined by Drude model [31]. Our study mainly focuses on the fundamental mode due to a vast majority of energy transmitted in the form of the fundamental mode. Based on confinement loss calculation method [32], the parameters such as spectral sensitivity, amplitude sensitivity, propagation length [27] and resolution are calculated.

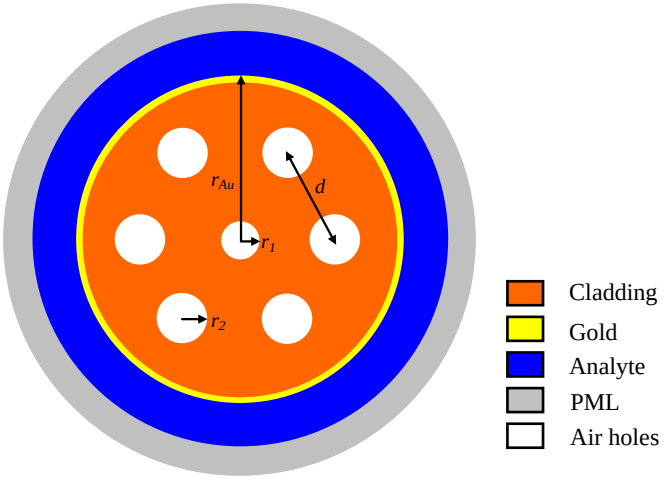

Fig. 1. Schematic diagram of the sensor.

3. Results and discussion

Fig. 2 shows the distribution of the effective index of the sensor. The blue curve shows the imaginary part of the refractive index of the fundamental mode and the black one represents the real part. Both of them depend on the wavelength. There is an obvious absorption peak at 825 nm due to coupling between the core-guided mode and excited plasmon mode.

In general, the geometric parameters influence the optical properties of the sensor and the thickness of the gold layer is one of the significant parameters. Fig. 3 shows the dependence of optical loss on the gold film thickness for different resonance wavelengths. The refractive index of the analyte is 1.39. The energy loss increases initially and then decreases with the gold layer thickness for each resonance wavelength, implying that the coupling depends on the gold film thickness and there is an optimal gold film thickness for each wavelength. It is consistent with the results obtained from the prism-coupled configuration [13]. The resonance depth decreases with wavelengths between 730 nm and 790 nm attributable to less energy penetration of the core mode electric field into the gold film as the wavelengths increase resulting in weak mode coupling. Moreover, the curves showing the dependence of energy loss broadens with increasing resonance wavelengths. It can be concluded that the strongest resonance can be excited at 730 nm and the optimal gold film thickness is 41 nm.

To determine the effects of the analyte channel width on the sensor performance, the analyte channel width is changed from 0.3 μm to 0.5 μm while the other parameters are kept the same.

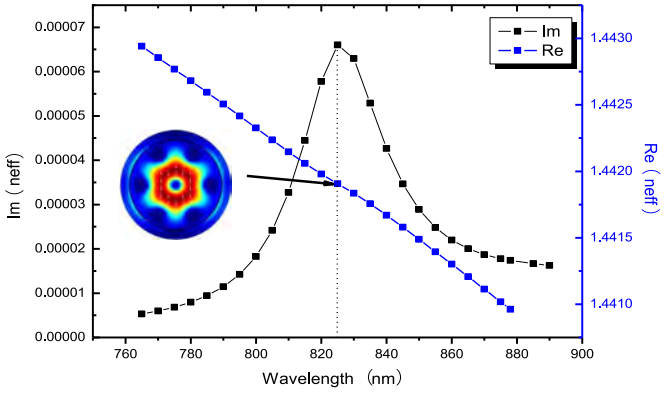

Fig. 2. Distribution of the effective index of the sensor. ($r_1=0.4$ μm, $r_2=0.6$ μm, $n=1.0$, $d=3$ μm, $t_{Au}=0.05$ μm, $n_{anal}=1.4$, $r_{Au}=4.05$ μm). (For interpretation of the references to color in this figure, the reader is referred to the web version of this article.)

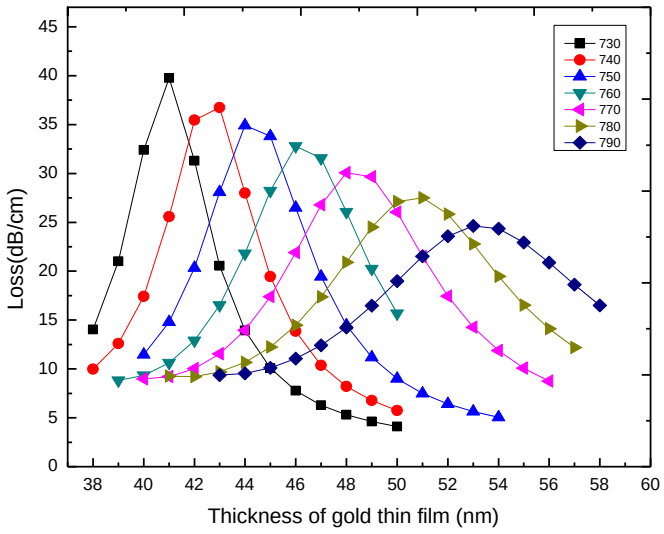

Fig. 3. Dependence of optical loss on the gold film thickness for different resonance wavelengths. (r_1=0.4 μm, r_2=0.6 μm, n=1.0, d=3 μm, n_{anal}=1.39).

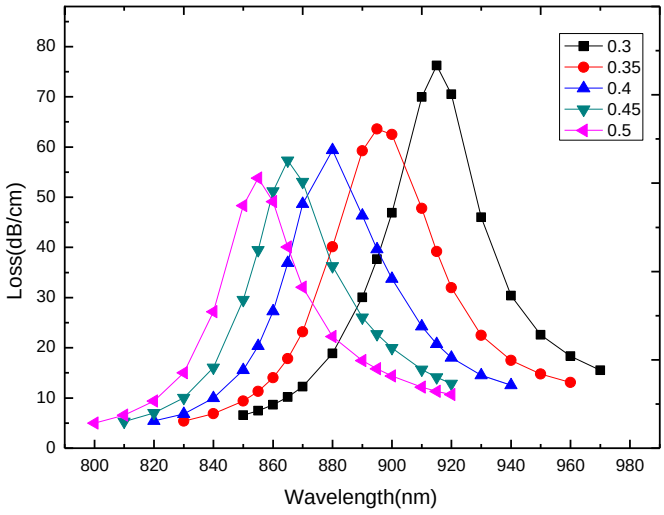

Fig. 4. Loss spectra of the sensors with different analyte channel widths. (r_1=0.4 μm, r_2=0.6 μm, n=1.0, d=3 μm, t_{Au}=0.05 μm, n_{anal}=1.41, r_{Au}=4.05 μm).

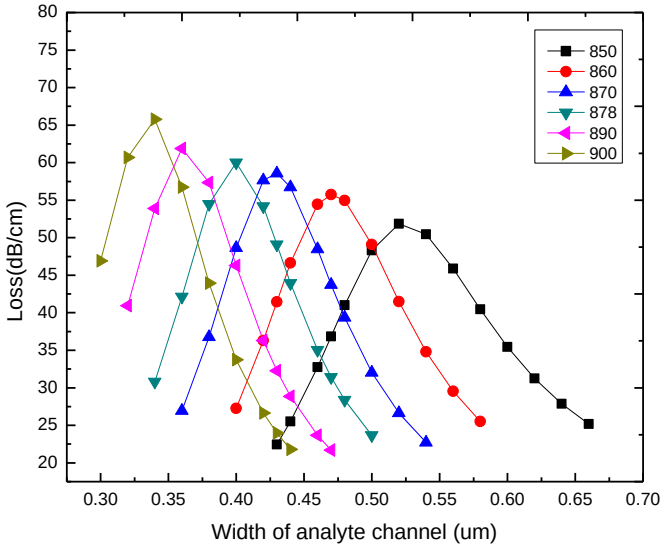

Fig. 5. Dependence of optical loss on the analyte channel width for different wavelengths. (r_1=0.4 μm, r_2=0.6 μm, n=1.0, d=3 μm, t_{Au}=50 nm, n_{anal}=1.41).

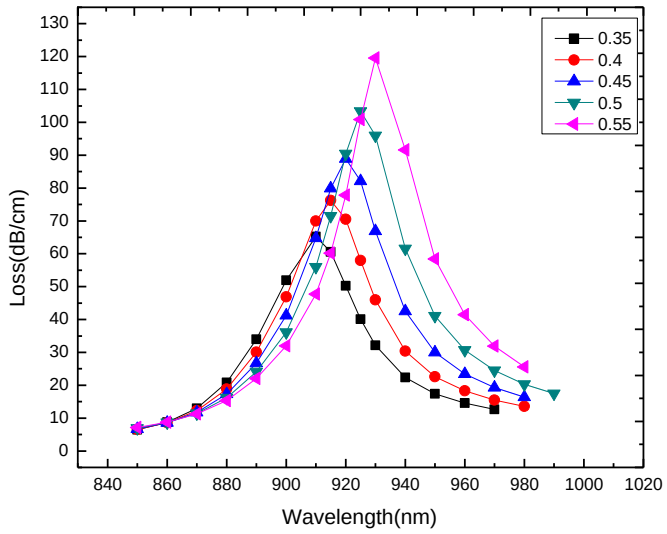

Fig. 6. Dependence of the loss spectra on the radius of the central air hole (r_2=0.6 μm, n=1.0, d=3 μm, t_{Au}=0.05 μm, n_{anal}=1.4, r_{Au}=4.05 μm).

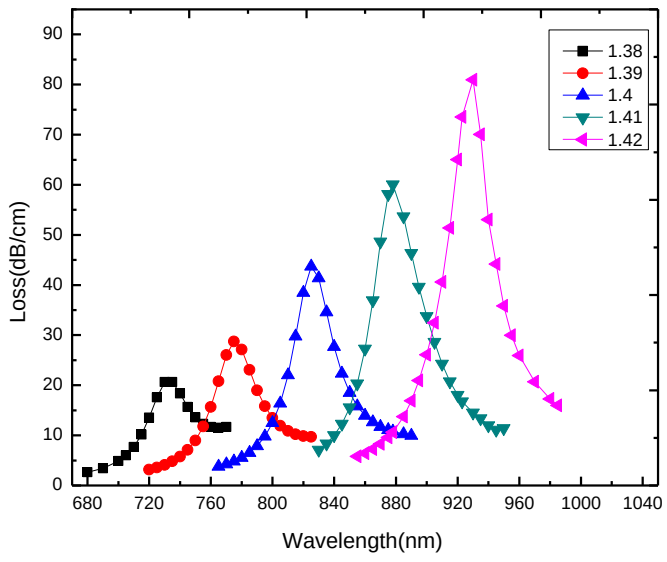

Fig. 7. Loss spectra of the fundamental mode for different analytes (r_1=0.4 μm, r_2=0.6 μm, n=1.0, d=3 μm, t_{Au}=0.05 μm, r_{Au}=4.05 μm).

Fig. 4 presents the loss spectra of the sensor with different analyte channel widths. The refractive index of the analyte is 1.41. The resonance depth of the loss spectra increases with the analyte channel width decreasing, indicating the light propagation in cladding decreases and the coupling between plasmonic mode and fundamental mode increases.

Fig. 5 shows the dependence of the optical loss on analyte channel width for different wavelengths. The optical loss for each curve rises initially reaching a maximum and then diminishes as the width of the analyte channel is increased. In addition, the curves shift towards larger analyte channel thickness as the wavelength is decreased. If the refractive index of the analyte is 1.41, stronger resonance is observed when the thickness of analyte channel and resonance wavelength is 0.34 μm and 900 nm, respectively. The curves showing the dependence of energy loss on analyte channel width broaden as the resonance wavelength decreases, indicating that phase matching between the core-guided mode and surface plasmon resonance mode can be achieved for a larger range of analyte channel. It is noteworthy that the result is only valid in a certain range of channel width, and it will be

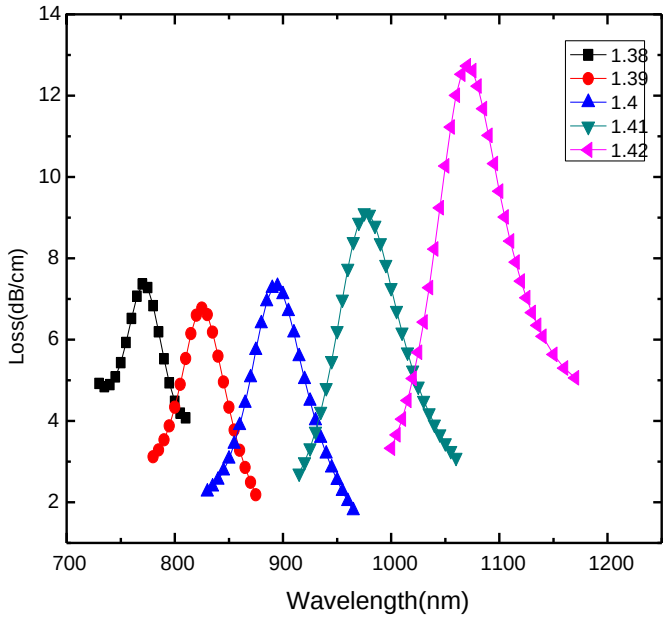

Fig. 8. Loss spectra of the fundamental mode for different analytes (r_1=0.4 μm, r_2=0.6 μm, n=1.0, d=3 μm, t_{Au}=0.05 μm, t_{Gra}=20 nm, r_{Au}=4.05 μm).

independent of the width for a large value of the analyte channel width.

The radius of the central air hole changes the refractive index of the fundamental core mode consequently affecting phase matching between the plasmon and core modes. Fig. 6 displays the dependence of the loss spectra on the radius of the central air hole. The resonance wavelengths red-shift and resonance amplitude increases with increasing radius, implying that the resonance wavelengths can be tailored by varying the size of the central air hole.

SPR is particularly sensitive to the surrounding dielectrics. In this work, the loss characteristics of the sensor are investigated for analyte refractive indexes between 1.38 and 1.42 and the results are presented in Fig. 7. The resonance strength increases with increasing refractive indexes and the resonance peak red-shifts. By detecting the changes in the resonance peak positions ($\Delta\lambda_{peak}$) and variations of the analyte refractive indexes (Δn_a), the spectral sensitivity can be calculated as follows [20]:

$$S(\lambda) = \frac{\Delta\lambda_{peak}}{\Delta n_a}\,(\mathrm{nm/RIU}) \tag{1}$$

Here, Δn_a is assumed to be 0.01, and the peak shift is about $\Delta\lambda_{peak}$=48.75 nm estimated from Fig. 7, a high spectral sensitivity of 4875 nm/RIU is achieved in the sensing range between 1.38 and 1.42. In order to obtain a higher sensing sensitivity, an extra graphene layer with a thickness of 20 nm is attempted to be deposited on the gold layer in the model. The loss spectra of the fundamental mode for different analytes are shown in Fig. 8. The resonance peaks shift to longer wavelengths when the refractive indexes of the analytes vary from 1.38 to 1.42. Furthermore, the spectral sensitivity is approximately 7500 nm/RIU for refractive indexes between 1.38 and 1.42, which is significantly increased due to the graphene addition.

The wavelength resolution is assumed to be $\Delta\lambda_{min}$=0.1 nm. The refractive index resolution of the proposed sensor can be defined as [33]:

$$R = \Delta n_a \Delta\lambda_{min}/\Delta\lambda_{peak} \tag{2}$$

Here, the peak shift is about $\Delta\lambda_{peak}$=48.75 nm estimated from Fig. 7. When the variation of the analyte refractive index is

Table 1
Key parameters associated with the sensing performance of sensors.

PCF structure	Detection RI range (RIU)	Operation wavelength range (nm)	Spectral sensitivity (nm/RIU)	Spectral resolution (RIU)	Amplitude sensitivity (RIU^{-1})	Amplitude resolution (RIU)	Propagation length (cm)	Ref.
Analyte-filled core	1.45–1.47	500–600	347	1×10^{-4}	–	–	–	[17]
Analyte-filled central core	1.33–1.42	475–750	2929	3.72×10^{-4}	–	–	0.1316	[18]
central analyte channel with silver and graphene	1.46–1.49	990–1200	2390	3.33×10^{-5}	418	2.4×10^{-5}	0.0965	[19]
Double-analyte-channels	1.33–1.42	450–800	2000	2.3×10^{-6}	323	3.1×10^{-5}	0.7869	[20]
Six analyte channels, Air hole in core	1.33–1.49	500–750	2083	5×10^{-6}	290	3.3×10^{-5}	0.0668	[21]
Multi-core, Analyte-filled central hole	1.41–1.42	650–840	3300	3.03×10^{-5}	570	1.74×10^{-5}	0.5869	[22]
Seven holes	RI for distilled water	623	4000	2.5×10^{-5}	2232.5	4.5×10^{-6}	0.00654	[26]
Twelve holes	RI for distilled or heavy water	618–651	5229	1.9×10^{-5}	3941.5	2.5×10^{-6}	0.00457	[27]
Outmost analyte channel, 50 nm Gold	1.38–1.42	700–1100	4875	2.5×10^{-5}	513	1.95×10^{-5}	0.0571	This work
Outmost analyte channel, 50 nm Gold, 20 nm Graphene	1.38–1.42	700–1100	7500	1.33×10^{-5}	375	2.67×10^{-5}	0.3341	This work

$\Delta n_a = 0.01$, a sensing resolution of 2.5×10^{-5} RIU is obtained for refractive indexes between 1.38 and 1.42. As shown in Fig. 8, the peak shift in loss spectra is about $\Delta\lambda_{peak} = 75$ nm after adding graphene, the variation of the analyte refractive index is $\Delta n_a = 0.01$, Assuming that a transmitted intensity of 1% can be detected reliably, a resolution of 1.33×10^{-5} RIU is accomplished.

To evaluate the performance of the proposed sensors, Table 1 lists the key parameters for the sensing performance of PCF-SPR sensors with different structures. By means of a detailed survey on theses sensors listed in Table 1, it is found that the performance of PCF-SPR sensors depends strongly on sensing structures. Different sensors exhibit a certain advantage over other sensors, for instance, the sensor in Ref. [27] possesses an amplitude sensitivity of 3941.5 RIU^{-1} and an amplitude resolution of 2.5×10^{-6} RIU. Compared with the specific data listed in Table 1, the proposed sensors in this work display prominent characteristics of the spectral sensitivities of 7500 nm/RIU, which may be attributed to the contribution of graphene layers and the feature of locating analyte channel on the outermost layer in the configuration. It has been demonstrated that the interference between neighboring channels can not be ignored when the analytes are infiltrated in several closely arranged cylindrical-metalized channels [18]. The sensors with the analyte channel on the outermost layer are inclined to eliminate the interference between neighboring channels in this work. Therefore, the stronger energy coupling between the plasmonic mode and core-guided mode can easily be achieved, leading to higher spectral sensitivities.

4. Conclusion

A PCF-based SPR sensor with seven air holes and annular analyte is designed. Since the curvature of the thin gold film is much smaller than the other sensors, it is easy to deposit the film. The sensor is evaluated numerically using COMSOL Multiphysics based on the finite element method and the performance of the sensor is found to depend on the structure. A high spectral sensitivity of 4875 nm/RIU is achieved and the amplitude sensitivity can be as high as 513 RIU^{-1}. Besides, an extra graphene layer with the thickness of 20 nm is deposited on gold thin film in the proposed model, up to 7500 nm/RIU spectral sensitivity is obtained.

Acknowledgments

This work was supported by the National Natural Science Foundation of China (Grant no. 51474069), Program for New Century Excellent Talents in Heilongjiang Provincial University (Granted no. 1253-NCET-002), China Postdoctoral Science Foundation Funded Project (Grant no. 2016M59150), Natural Science Foundation of Heilongjiang Province (Grant no. E2016007).

References

[1] Yanyan Huo, Tianqing Jia, Yi Zhang, Hua Zhao, Shian Zhang, Donghai Feng, Zhenrong Sun, Narrow and deep fano resonances in a rod and concentric square ring-disk nanostructures, Sensors 13 (9) (2013) 11350–11361.
[2] H. Zhao, Y.Y. Huo, T.Q. Jia, D.H. Feng, S.A. Zhang, Z.R. Sun, Plasmon ruler based on Fano resonance of a square ring-disk trimer nanostructures, Indian J. Phys. 89 (9) (2015) 931–936.
[3] Y.Y. Huo, T.Q. Jia, Y. Zhang, H. Zhao, S.A. Zhang, D.H. Feng, Z.R. Sun, Spaser based on Fano resonance in a rod and concentric square ring-disk nanostructure, Appl. Phys. Lett. 104 (11) (2014) 1–3.
[4] Wang Chi, Wu Yanni, Zheng Hairong, Li Caixia, Li Junna, Dong Jun, Generation of high-order resonance modes in visible and near-infrared range from square ring-disk system, Plasmonics 10 (6) (2015) 1915–1920.
[5] A.L. Washburn, L.C. Gunn, R.C. Bailey, Label-free quantitation of a cancer biomarker in complex media using silicon photonic microring resonators, Anal. Chem. 81 (22) (2009) 9499–9506.
[6] Chen Bing, Liu Chunliang, Si Jinhai, Design of broadband power splitters using two-mode interference in slot waveguides, Opt. Commun. 355 (2015) 367–375.
[7] T. Claes, J.G. Molera, K. De Vos, E. Schacht, R. Baets, P. Bienstman, Label-free biosensing with a slotwaveguide-based ring resonator in silicon on insulator, IEEE Photon. J. 1 (3) (2009) 197–204.
[8] R.A. Abram, S. Brand, Some theory of a dual-polarization interferometer for sensor applications, J. Phys. D: Appl. Phys. 48 (12) (2015) 125101–125113.
[9] Jiangtao Zhou, Yiping Wang, Changrui Liao, Bing Sun, Jun He, Guolu Yin, Shen Liu, Zhengyong Li, Guanjun Wang, Xiaoyong Zhong, Jing Zhao, Intensity modulated refractive index sensor based on optical fiber Michelson interferometer, Sens. Actuators B: Chem. 208 (2015) 315–319.
[10] Kai Ni, Tao Li, Limin Hu, Wenwen Qian, Quanyao Zhang, Shangzhong Jin, Temperature-independent curvature sensor based on tapered photonic crystal fiber interferometer, Opt. Commun. 285 (24) (2012) 5148–5150.
[11] J. Gabriel Ortega-Mendoza, Alfonso Padilla-Vivanco, Carina Toxqui-Quitl, Placido Zaca-Morán, David Villegas-Hernández, Fernando Chávez, Optical fiber sensor based on localized surface plasmon resonance using silver nanoparticles photodeposited on the optical fiber end, Sensors 14 (2014) 18701–18710.
[12] Violeta Marquez-Cruz, Jacques Albert, High resolution NIR TFBG-assisted biochemical sensors, J. Lightw. Technol. 33 (16) (2015) 3363–3373.
[13] E. Wijaya, Cédric Lenaerts, Sophie Maricot, Juriy Hastanin, Serge Habraken, Jean-Pierre Vilcot, Rabah Boukherroub, Sabine Szunerits, Surface plasmon resonance-based biosensors: from the development of different SPR structures to novel surface functionalization strategies, Curr. Opin. Solid State Mater. Sci. 15 (2011) 208–224.
[14] Jitendra Narayan Dash, Rajan Jha, Graphene based birefringent photonic crystal fiber sensor using surface plasmon resonance, IEEE Photon. Technol. Lett. 26 (2014) 1092–1095.
[15] A. Hassani, M. Skorobogatiy, Design of the microstructured optical fiber-based surface plasmon resonance sensors with enhanced microfluidics, Opt. Express 14 (24) (2006) 11616–11621.
[16] A. Hassani, M. Skorobogatiy, Photonic crystal fiber-based plasmonic sensors for the detection of bio-layer thickness, J. Opt. Soc. Am. B Opt. Phys. 26 (8) (2009) 1550–1557.
[17] M. Hautakorpi, M. Mattinen, H. Ludvigsen, Surface-plasmon-resonance sensor based on three-hole microstructured optical fiber, Opt. Express 16 (12) (2008) 8427–8432.
[18] Binbin Shuai, Li Xia, Yating Zhang, Deming Liu, A multi-core holey fiber based plasmonic sensor with large detection range and high linearity, Opt. Express 20 (2012) 5974–5986.
[19] A.A. Rifat, G.A. Mahdiraji, D.M. Chow, Y.G. Shee, R. Ahmed, F.R.M. Adikan, Photonic crystal fiber-based surface plasmon resonance sensor with selective analyte channels and graphene-silver deposited core, Sensors 15 (2015) 11499–11510.
[20] C. Zhou, Theoretical analysis of double-microfluidic-channels photonic crystal fiber sensor based on silver nanowires, Opt. Commun. 288 (2013) 42–46.
[21] P.B. Bing, J.Q. Yao, Y. Lu, Z.Y. Li, A surface-plasmon- resonance sensor based on photonic-crystal-fiber with large size microfluidic channels, Opt. Appl. (3) (493–501).
[22] P.P. Zhang, A surface plasmon resonance sensor based on a multi-core photonic crystal fiber, Opt. Lett. 35 (6) (2013) 1673–1682.
[23] Emmanuel K. Akowuah, Terry Gorman, Huseyin Ademgil, Shyqyri Haxha, Gary K. Robinson, Jenny V. Oliver, Numerical analysis of a photonic crystal fiber for biosensing applications, IEEE J. Quantum Electron. 48 (11) (2012) 1403–1410.
[24] R. Otupiri, E.K. Akowuah, S. Haxha, Senior Member, A novel birefrigent photonic crystal fiber surface plasmon resonance biosensor, IEEE Photon. J. 6 (4) (2014) 1–11.
[25] Yong Zhao, Ze-qun Deng, Jin Li, Photonic crystal fiber based surface plasmon resonance chemical sensors, Sens. Actuators B: Chem. 202 (2014) 557–567.
[26] V.A. Popescu, N.N. Puscas, G. Perrone, Power absorption efficiency of a new microstructured plasmon optical fiber, J. Opt. Soc. Am. B 29 (11) (2012) 3039–3046.
[27] V.A. Popescu, N.N. Puscas, G. Perrone, Strong power absorption in a new microstructured holey fiber-based plasmonic sensor, J. Opt. Soc. Am. B 31 (5) (2014) 1062–1070.
[28] Henri Jussila, He Yang, Niko Granqvist, Zhipei Sun, Surface plasmon resonance for characterization of large-area atomic-layer graphene film, Optica 3 (2) (2016) 151–158.
[29] J.K. Nayak, P. Parhi, R. Jha, Graphene oxide encapsulated gold nanoparticle based stable fibre optic sucrose sensor, Sens. Actuators B: Chem. 221 (2015) 835–841.
[30] K. Saitoh, M. Koshiba, Full-vectorial imaginary-distance beam propagation method based on a finite element scheme: application to photonic crystal fibers, IEEE J. Quantum Electron. 38 (7) (2002) 927–938.
[31] P.B. Johnson, R.W. Christy, Optical constants of the noble metals, Phys. Rev. B 6 (12) (1972) 682–687.
[32] Y. Cui, S. Heilshorn, L. Hu, A. Schoen, D. Schoen, Water Sterilization Devices Including Nanostructures and Uses Thereof, US Patent WO2011/1339323A2, April 22, 2011.
[33] D. Gao, C.Y. Guan, Y.W. Wen, X. Zhong, L.B. Yuan, Multi-hole fiber based surface plasmon resonance sensor operated at near-infrared wavelengths, Opt. Commun. 313 (2014) 94–98.